SEPT Vibration Test Report Preliminary

V1.0

Prepared by:

L. Duvet, ESTEC

R. Mueller-Mellin, University of Kiel

S. Boettcher, University of Kiel

Doc. No.: STEREO-ETKI-011

February 2004

Table of contents

List of figures

1 Objectives

The purpose of this document is to give a preliminary analysis of the results of the SEPT vibration tests which occurred at ESA/ESTEC from February 16 to 24, 2004. An official report (RD1) will be issued later by the facility.

2 Applicable Documents

AD1 SEPT vibration test plan, STEREO-ETKI-005, January 2004
AD2 SEPT Comprehensive Performance Test, STEREO-ETKI-009, January 2004
AD3 STEREO Environment Definition, Observatory, Component and Instrument Test Requirements Document, Doc. No. 7381-9003
AD4 STEREO Contamination Control Plan, Doc. No. 7381-9006
AD5 IMPACT Environmental Test Plan, Version D 2003-Dec-30
AD6 IMPACT Contamination Control Plan, Version A 2003-May-14

3 Reference documents

RD1 SEPT Vibration Test Facility Data Report, to be released
RD2 STEREO SEPT Structural Analysis TOS-MCS/2002/721/ln, January 2003
RD3 Validation of Force Limited Vibration Testing at NASA Langley Research Center, C.E. Rice, R. D. Buehrle, NASA/TM-2003-212404, May 2003
RD4 Reduction of Overstesting during vibration tests of space hardware, Y. Soucy, A. Cote, Vol. 48, No. 1, March 2002, Canadian Aeronautics and Space Journal

4 Acronyms and Abbreviations

EGSE	Electrical Ground Support Equipment
FPGA	Field Programmable Gate Array
PDFE	Particle Detector Front End
PIPS	Passivated Ion-implanted Planar Silicon detector
PSD	Power Spectrum Density
SEPT-E	Solar Electron and Proton Telescope – Ecliptic
SEPT-NS	Solar Electron and Proton Telescope – North/South
SSD	Solid State Detector

5 Overview

5.1 Set-up

The shaker is located at ESA/ESTEC (Netherlands) and is shown in Fig. 1:

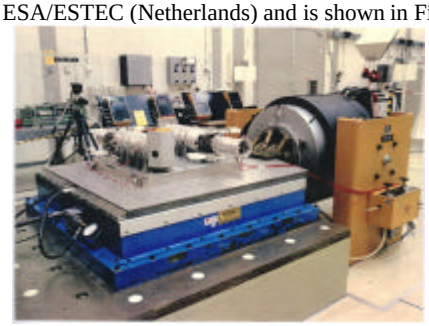

Figure 1: 70 kN shaker in the horizontal position

For the SEPT vibration tests, the configuration was as follows:

- The 70 kN shaker was placed in a vertical position (w.r.t. the position shown in Fig. 1.)
- An aluminium cube of ~ 250 mm side length was used to support two flight units
- By changing the faces on which the units are mounted, a different axis was stimulated
- No counterweight was used
- SEPT-E with Ultem bushings was mounted to the cube with fasteners M4 V2A (torque 2.6 Nm), mass 770g
- SEPT-NS with Ultem bushings was mounted to the bracket which in turn was mounted to the cube with fasteners M5 V2A (torque 5.1 Nm), mass 1110 g.

Some examples of configurations of the units on the shaker are shown in Fig. 2.

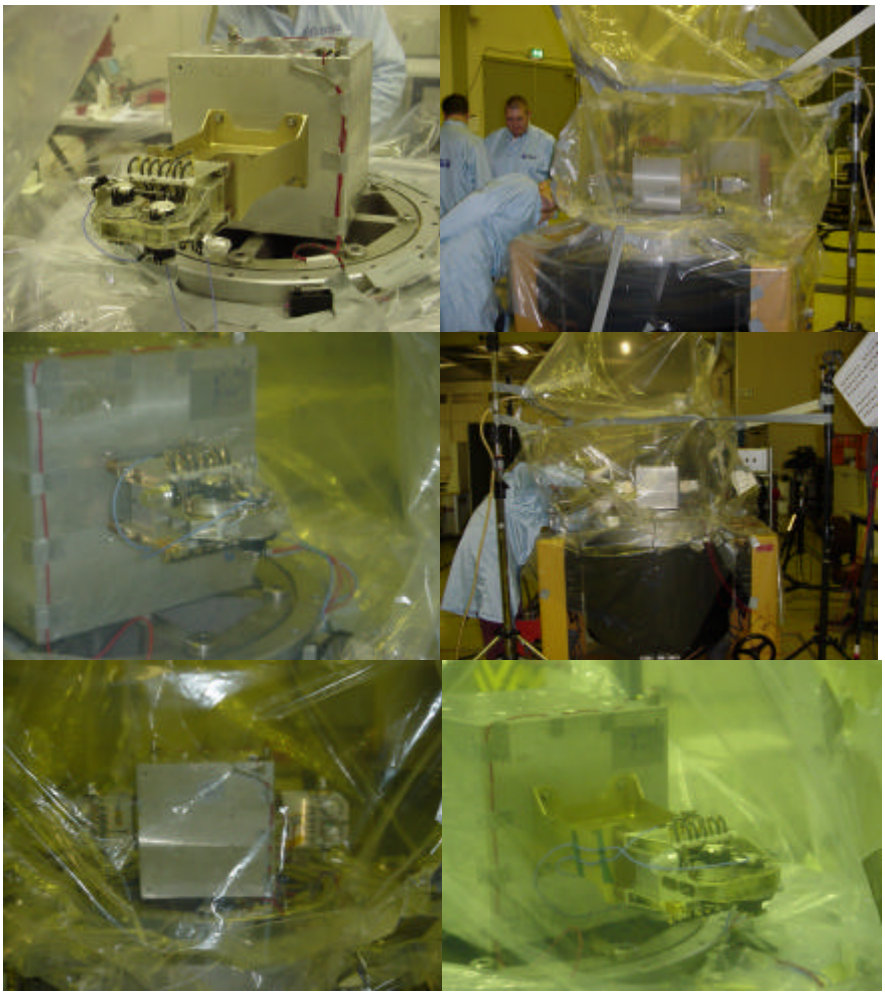

Figure 2: Configuration examples of the units

The instruments were constantly bagged during tests and purged with Nitrogen (Class5, 99.999% purity). One plastic foil was used to cover the shaker. A second plastic foil was taped to the top of the shaker so as to form a protective envelope maintained at the top by a small crane (see Fig. 3).

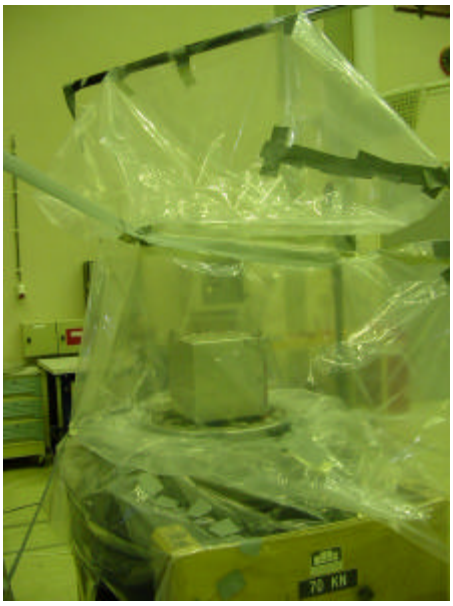

Figure 3: Protection bag during tests

For transport between the shaker facility and clean bench where the CPTs were carried out, the units were enclosed in a custom made Plexiglass container protected in an aluminium box (see Fig.4).

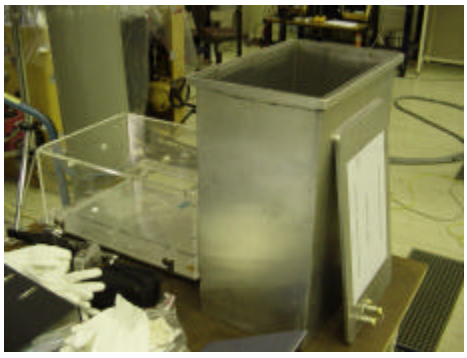

Figure 4: Transport container

5.1.1 Axis definition

The sketches in Fig. 5 show the definition of the three axes for SEPT.

SEPT-E

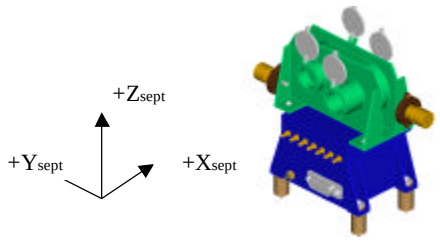

SEPT-NS

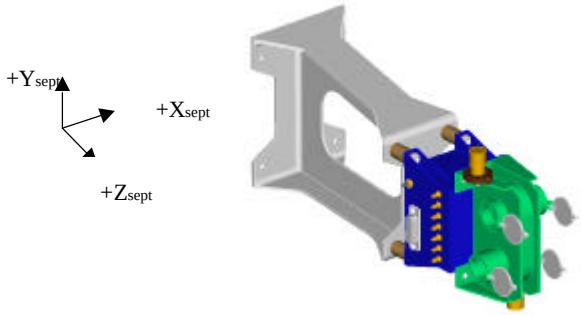

Figure 5: SEPT axis definition

5.1.2 Accelerometers

Two tri-axial accelerometers were used per unit, one placed on the sensor head (TP1), one placed on the electronics box (TP2). The accelerometers were placed on identical positions on corresponding FM1 and FM2 units:

- For FM1, the accelerometers are placed on the MDM connector side.
- For FM2, the accelerometers are placed on the S/C temperature connector side.

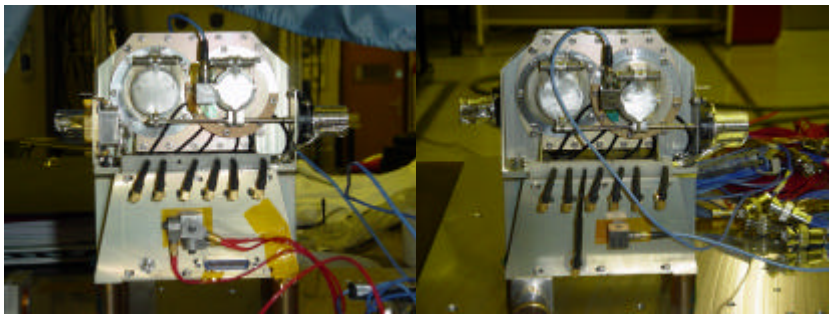

Figure 6: Position of the accelerometers on a unit (in that case SEPT-E, FM1 and FM2)

The accelerometers were glued on a Kapton tape previously applied at the chosen location. Two tri-axial reference accelerometers were also placed on the cube („Pilot“) to control the input.
Table 1 shows the names and location of the accelerometers:

Channel	Type	Point Id	Transducer Id	Position
1	Control	P1z	RP85	Cube upper face
2	Control	P2z	NB52	
3	Measure	CP1Y	BE55	
4	Measure	CP1X	DH93	
5	Measure	FM1_TP1X	23652Z	FM1-E/NS sensor head
6	Measure	FM1_TP1Y	23652Y	
7	Measure	FM1_TP1Z	23652X	
8	Measure	FM1_TP2X	BE62	FM1-E/NS electronics box
9	Measure	FM1_TP2Y	BM40	
10	Measure	FM1_TP2Z	BON3	
11	Measure	FM2_TP1X	24397Z	FM2-E/NS sensor head
12	Measure	FM2_TP1Y	24397Y	
13	Measure	FM2_TP1Z	24397X	
14	Measure	FM2_TP2X	23654Z	FM2-E/NS electronics box
15	Measure	FM2_TP2Y	23654X	
16	Measure	FM2_TP2Z	23654Y	

Table 1:Accelerometer description

5.2 Test sequence

The reference test sequence is shown in Table 2.

Run #	Data log name	Level	Unit and axis	Position on the cube
1	FM1-E-SL-X-1	Sine-Low	FM1 SEPT-E X_{sept} axis	One unit on each of the two lateral sides
	FM2-E-SL-X-1	Sine-Low	FM2 SEPT-E X_{sept} axis	

2	FM1-E-ST-X	Sine-Thrust	FM1 SEPT-E X_{sept} axis	One unit on each of the two lateral sides
	FM2-E-ST-X	Sine-Thrust	FM2 SEPT-E X_{sept} axis	
3	FM1-E-SL-X-2	Sine-Low	FM1 SEPT-E X_{sept} axis	One unit on each of the two lateral sides
	FM2-E-SL-X-2	Sine-Low	FM2 SEPT-E X_{sept} axis	
4	FM1-E-RPar-X	Random-Parallel	FM1 SEPT-E X_{sept} axis	One unit on each of the two lateral sides
	FM2-E-RPar-X	Random-parallel	FM2 SEPT-E X_{sept} axis	
5	FM1-E-SL-X-3	Sine-Low	FM1 SEPT-E X_{sept} axis	One unit on each of the two lateral sides
	FM2-E-SL-X-3	Sine-Low	FM2 SEPT-E X_{sept} axis	
6	FM1-NS-SL-X-1	Sine-low	FM1 SEPT-NS X_{sept} axis	One unit on each of the two lateral sides
	FM2-NS-SL-X-1	Sine-low	FM2 SEPT-NS X_{sept} axis	
7	FM1-NS-SLat-X	Sine-lateral	FM1 SEPT-NS X_{sept} axis	One unit on each of the two lateral sides
	FM2-NS-SLat-X	Sine-lateral	FM2 SEPT-NS X_{sept} axis	
8	FM1-NS-SL-X-2	Sine-low	FM1 SEPT-NS X_{sept} axis	One unit on each of the two lateral sides
	FM2-NS-SL-X-2	Sine-low	FM2 SEPT-NS X_{sept} axis	
9	FM1-NS-RPar-X	Random-parallel	FM1 SEPT-NS X_{sept} axis	One unit on each of the two lateral sides
	FM2-NS-Rpar-X	Random-parallel	FM2 SEPT-NS X_{sept} axis	
10	FM1-NS-SL-X-3	Sine-low	FM1 SEPT-NS X_{sept} axis	One unit on each of the two lateral sides
	FM2-NS-SL-X-3	Sine-low	FM2 SEPT-NS X_{sept} axis	
11	FM1-E-SL-Y-1	Sine-Low	FM1 SEPT-E Y_{sept} axis	One unit on each of the two lateral sides
	FM2-E-SL-Y-1	Sine-Low	FM2 SEPT-E Y_{sept} axis	
12	FM1-E-ST-Y	Sine-thrust	FM1 SEPT-E Y_{sept} axis	One unit on each of the two lateral sides
	FM2-E-ST-Y	Sine-thrust	FM2 SEPT-E Y_{sept} axis	
13	FM1-E-SL-Y-2	Sine-Low	FM1 SEPT-E Y_{sept} axis	One unit on each of the two lateral sides
	FM2-E-SL-Y-2	Sine-Low	FM2 SEPT-E Y_{sept} axis	
14	FM1-E-RPar-Y	Random-parallel	FM1 SEPT-E Y_{sept} axis	One unit on each of the two lateral sides
	FM2-E-Rpar-Y	Random-parallel	FM2 SEPT-E Y_{sept} axis	
15	FM1-E-SL-Y-3	Sine-Low	FM1 SEPT-E Y_{sept} axis	One unit on each of the two lateral sides
	FM2-E-SL-Y-3	Sine-Low	FM2 SEPT-E Y_{sept} axis	
16	FM1-NS-SL-Y-1	Sine-low	FM1 SEPT-NS Y_{sept} axis	One unit on

	FM2-NS-SL-Y-1	Sine-low	FM2 SEPT-NS Y_{sept} axis	each of the two lateral sides
17	FM1-NS-ST-Y	Sine-thrust	FM1 SEPT-NS Y_{sept} axis	One unit on each of the two lateral sides
	FM2-NS-ST-Y	Sine-thrust	FM2 SEPT-NS Y_{sept} axis	
18	FM1-NS-SL-Y-2	Sine-low	FM1 SEPT-NS Y_{sept} axis	One unit on each of the two lateral sides
	FM2-NS-SL-Y-2	Sine-low	FM2 SEPT-NS Y_{sept} axis	
19	FM1-NS-RPar-Y	Random-parallel	FM1 SEPT-NS Y_{sept} axis	One unit on each of the two lateral sides
	FM2-NS-RPar-Y	Random-parallel	FM2 SEPT-NS Y_{sept} axis	
20	FM1-NS-SL-Y-3	Sine-low	FM1 SEPT-NS Y_{sept} axis	One unit on each of the two lateral sides
	FM2-NS-SL-Y-3	Sine-low	FM2 SEPT-NS Y_{sept} axis	
21	FM1-E-SL-Z-1	Sine-Low	FM1 SEPT-E Z_{sept} axis	Both units on on +Zshaker face
	FM2-E-SL-Z-1	Sine-Low	FM2 SEPT-E Z_{sept} axis	
22	FM1-E-SLat-Z	Sine-Lateral	FM1 SEPT-E Z_{sept} axis	Both units on on +Zshaker face
	FM2-E-SLat-Z	Sine-Lateral	FM2 SEPT-E Z_{sept} axis	
23	FM1-E-SL-Z-2	Sine-Low	FM1 SEPT-E Z_{sept} axis	Both units on on +Zshaker face
	FM2-E-SL-Z-2	Sine-Low	FM2 SEPT-E Z_{sept} axis	
24	FM1-E-RPerp-Z	Random-perpendicular	FM1 SEPT-E Z_{sept} axis	Both units on the +Zshaker face
	FM2-E-RPerp-Z	Random-perpendicular	FM2 SEPT-E Z_{sept} axis	
25	FM1-E-SL-Z-3	Sine-Low	FM1 SEPT-E Z_{sept} axis	Both units on on +Zshaker face
	FM2-E-SL-Z-3	Sine-Low	FM2 SEPT-E Z_{sept} axis	
26	FM1-NS-SL-Z-1	Sine-low	FM1 SEPT-NS Z_{sept} axis	Both units on the +Zshaker face
	FM2-NS-SL-Z-1	Sine-low	FM2 SEPT-NS Z_{sept} axis	
27	FM1-NS-SLat-Z	Sine-lateral	FM1 SEPT-NS Z_{sept} axis	Both units on the +Zshaker face
	FM2-NS-SLat-Z	Sine-lateral	FM2 SEPT-NS Z_{sept} axis	
28	FM1-NS-SL-Z-2	Sine-low	FM1 SEPT-NS Z_{sept} axis	Both units on the +Zshaker face
	FM2-NS-SL-Z-2	Sine-low	FM2 SEPT-NS Z_{sept} axis	
29	FM1-NS-RPerp-Z	Random-perpendicular	FM1 SEPT-NS Z_{sept} axis	Both units on the +Zshaker face
	FM2-NS-Rperp-Z	Random-perpendicular	FM2 SEPT-NS Z_{sept} axis	
30	FM1-NS-SL-Z-3	Sine-low	FM1 SEPT-NS Z_{sept} axis	Both units on the +Zshaker face
	FM1-NS-SL-Z-3	Sine-low	FM2 SEPT-NS Z_{sept} axis	

Table 2: Test sequence

As the SEPT-NS units were available earlier, it was decided to start with them (Run #6). To improve safety margin a low level random (-12 dB w.r.t. specified random levels, see RD1) was carried out each time before the full level random. Besides some additional low level sine sweeps were needed in order to tune the model presented in RD2 and improve our understanding of the results.

6 Results

6.1 Overview

The tests were performed as expected, but some points require additional explanation:

- axes cross-talk
- resonance frequency shift for SEPT-NS units
- FM1 / FM2 level response differences
- Active notching
- Torque influence

6.1.1 Axes cross-talk

The cross-talk between the different axes is due to the fact that the centre of gravity of the units are not ideally located w.r.t. the main axis of the cube. As a consequence, the shaker slightly stimulates the units in the axes perpendicular to the axis under test.

6.1.2 Resonance frequency shift for SEPT-NS

The simulation model (see RD2) initially showed a fundamental eigen frequency of 66 Hz while the first resonance frequency of the test showed 115 Hz. This factor of 2 discrepancy was not present for SEPT-E, which leads naturally to think that the bracket was the cause. Indeed, the main difference between the model and the test is the possibility for the modelled base of the bracket to move non-negligibly whereas on the cube, the large contact surface between the bracket base and the cube prevents this behaviour and therefore increases the overall stiffness. This parameter was introduced in a new simulation which confirms the above hypothesis because the results now fit within 10 % the observed resonance frequencies (see Figure 7 and Figure 8). This result also points out the problem of over-testing of flight units (see RD3, RD4).

The model could be further improved by refining the Ultem bushing properties. Note that 4 safety nuts were added to SEPT-NS for the fasteners between the electronics box and the bracket (the nuts were not staked). The nut was part of our original design, but was first left out because the bracket was delivered unexpectedly with threaded holes.

6.1.3 Resonance output level differences

At many occasions, the output level of a FM1 unit was different from the FM2 unit even though the units NS and E are almost perfectly identical. This “paradox” can be solved when looking at the ratio output/input level for each unit, which constitutes the real signature of the instrument (Q factor at resonance). The following example illustrates this problem. The two units SEPT-E were tested along the X axis with a sine sweep (see Figure 12 in the appendix). Table 3 summarizes the results:

Unit	Resonance frequency (Hz)	Input level (g)	Output level (g)	Q factor
FM1	418	0.365	28.3	77
FM2	422	0.265	18.5	70

Table 3: Example of response analysis

The output levels differ greatly but so do the input levels, indeed the shaker operates in a closed loop with the pilot accelerometers such that the input level remains around 0.25g (+/- 3dB). The variations are partly due to the limited response time of the closed loop system. The Q factors for both units differ only by 10 %, which is more than reasonable and confirms the similarity of the units.

6.1.4 Active notching

Active notching consists in observing in real time the output PSD and limiting it to a chosen value in a narrow frequency band. For each random sequence a low level random was initially performed. In a second step, from the PSD response and the corresponding rms value, we calculated the maximum safe PSD at full level. Our main criterion was to limit the overall rms value to 50 g rms corresponding to a safety margin factor of 3.7 (see RD2). Test results indicate whether an actual notching has occurred via the so-called “Error spec” curves (see Figure 13 in the appendix) which gives the deviation from the specified input PSD. Note that unless the notching is strong (< -3dB) it is difficult to separate it from the natural shaker uncertainty. The maximum notching observed was -2.57 dB at 415 Hz on the X-axis of SEPT-E (see Fig. 13).

6.1.5 Torque influence

Both types of units were torqued on the cube using a torque-meter: 2.6 Nm for SEPT-E, 5.1 Nm for SEPT-NS.

At the end of each axis test, the torque (to unscrew) was measured. On average, the torque at the end was 20 % lower than the initial torque. On one occasion, it was possible to observe a shift (toward a lower value) of the resonance frequencies after the random run (SEPT-NS, X axis). By reapplying the proper torque, the frequency shift vanished for one of the model and went even above the original value for the other. This test clearly showed that torque values were essential in the resonance frequency determination of SEPT-NS. This point also strongly supports the hypothesis developed in section 6.1.2 concerning the interface between the bracket base and the cube.

The following sections will detail the results obtained in the different configurations. Some selected plots are presented as reference in the appendix. All the results and plots will be available in RD1.

6.2 SEPT-NS

6.2.1 X axis

Unit	Sine sweep			Random	
	1st Resonance frequency (Hz)		Max g	Max g rms	Remark
	Simulation	Test			
FM1	66.39 * 127.79 **	~115	20.63 (TP1)	26.06 (TP1)	-1 dB error at resonance
FM2	66.39* 127.79**	~115	12.07 (TP1)	20.64 (TP1)	

Table 4: SEPT-NS X axis main results

* according to RD2
** Vibration test simulation (see below)

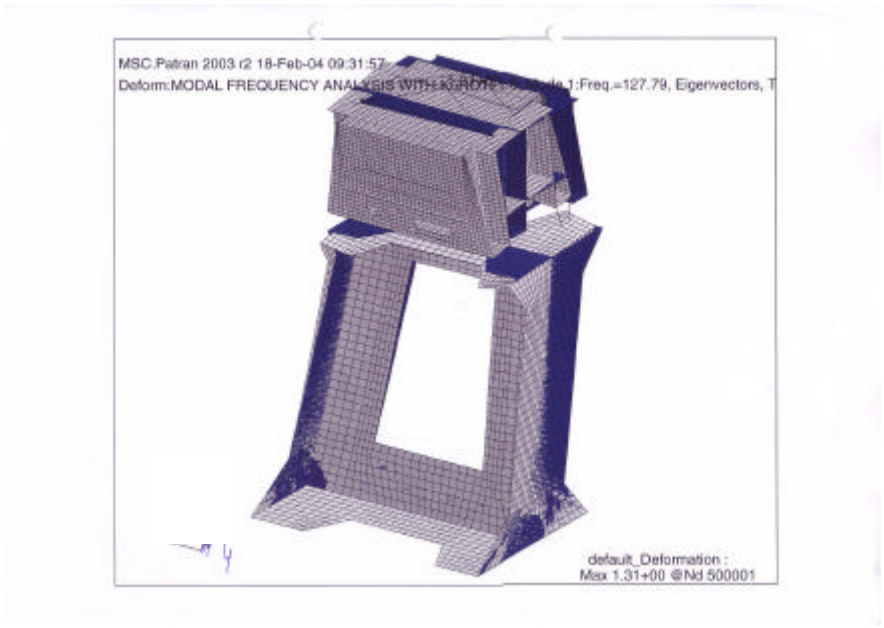

Figure 7: Vibration test simulation (X axis)

Sine high level test (5-100 Hz) was performed successfully.

6.2.2 Y axis

Unit	Sine sweep			Random	
	1st Resonance frequency (Hz)		Max g	Max g rms	Remark
	Simulation	Test			
FM1	114.26 * 231.87**	~220	8.77 (TP1)	27.11 (TP1)	-1.53 dB error at resonance
FM2	114.26* 231.87**	~250	6.82 (TP1)	17.67 (TP1)	

Table 5: SEPT-NS Y axis main results

* according to RD2
** Vibration test simulation (see below)

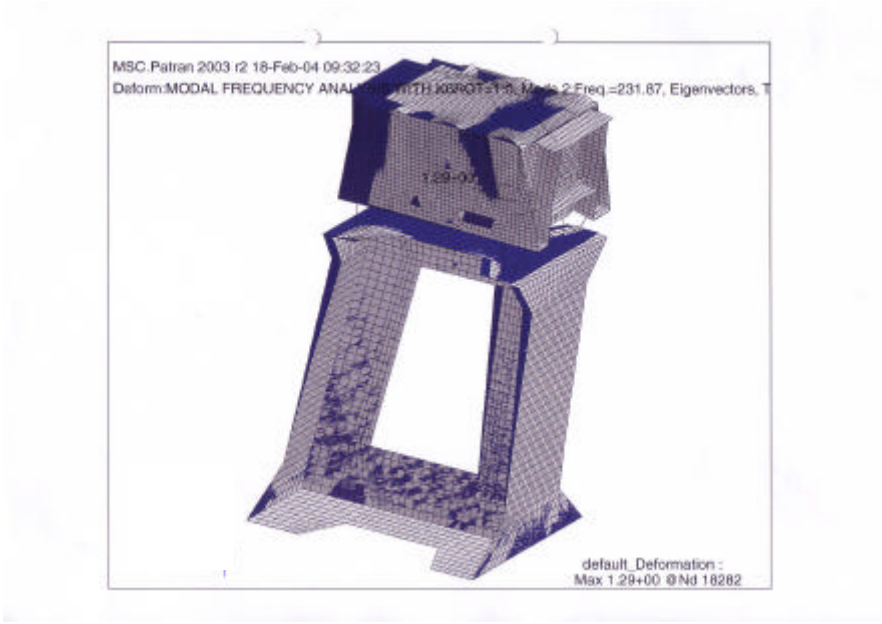

Figure 8: Vibration test simulation (Y axis)

Sine high level test (5-100 Hz) was performed successfully.

6.2.3 Z axis

Unit	Sine sweep			Random	
	1st Resonance frequency (Hz)		Max g	Max g rms	Remark
	Simulation	Test			
FM1	362.68 * 600 and 700 **	~710	5.79 (TP1)	40.9	-1.1 dB error at resonance
FM2	362.68* 600 and 700 **	~710	11.37 (TP1)	49.94	

Table 6: SEPT-NS Z axis main results

* according to RD2
** Vibration test simulation
Sine high level test (5-100 Hz) was performed successfully.

6.3 SEPT-E

6.3.1 X axis

Unit	Sine sweep			Random	
	1st Resonance frequency (Hz)		Max g	Max g rms	Remark
	Simulation	Test			
FM1	451.52	422	28.56 (TP1)	44.43	–2.57 dB error at resonance
FM2	451.52	418	19.44 (TP1)	39.57	

Table 7: SEPT-E X axis main results

Sine high level test (5-100 Hz) was performed successfully.

6.3.2 Y axis

Unit	Sine sweep			Random	
	1st Resonance frequency (Hz)		Max g	Max g rms	Remark
	Simulation	Test			
FM1	436.02	470	10.96 (TP1)	25.01	No notching
FM2	436.02	500	6.68 (TP1)	28.49	

Table 8: SEPT-E Y axis main results

Sine high level test (5-100 Hz) was performed successfully.

6.3.3 Z axis

Unit	Sine sweep			Random	
	1st Resonance frequency (Hz)		Max g	Max g rms	Remark
	Simulation	Test			
FM1	1144.88	1700 (other peak at 1100) on TP1	9.08	36.53	No notching
FM2	1144.88	1700 (other peak at 1100) on TP2	9.78	37.01 (on TP2)	

Table 9: SEPT-E Z axis main results

Sine high level test (5-100 Hz) was performed successfully.

The 1700 Hz peak is not foreseen by the simulation. For this axis, internal cabling, which may differ from unit to another and that is not taken into account in the model, could play a role at this high frequency. It has to be noted that the internal cabling is really different for SEPT-E and SEPT-NS, which may explain why the 1700 Hz peak is not visible for SEPT-NS (a peak is present at 1500 Hz).

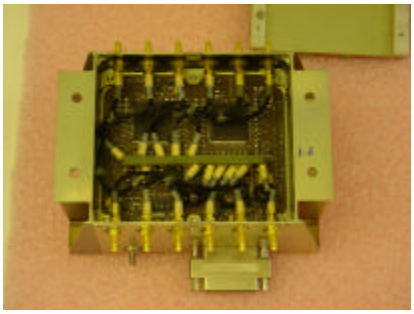

Figure 9: Internal cabling (a rectangular piece of epoxy is glued on top of the MMCX PCB connector to improve stiffness).

6.4 CPT results

A CPT (see AD2) was carried out each time an axis change occurred. A Co60 detector aliveness test was included. All CPT's were successful.

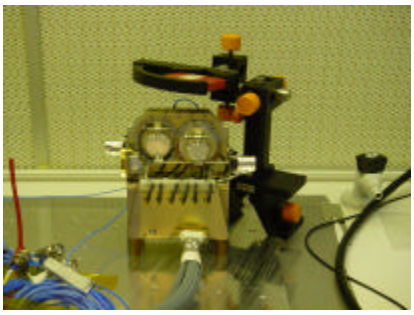

Figure 10: Typical configuration during CPT with Co60 source

6.5 Pinpuller tests

A pinpuller test was performed before and after a unit has been fully vibrated.

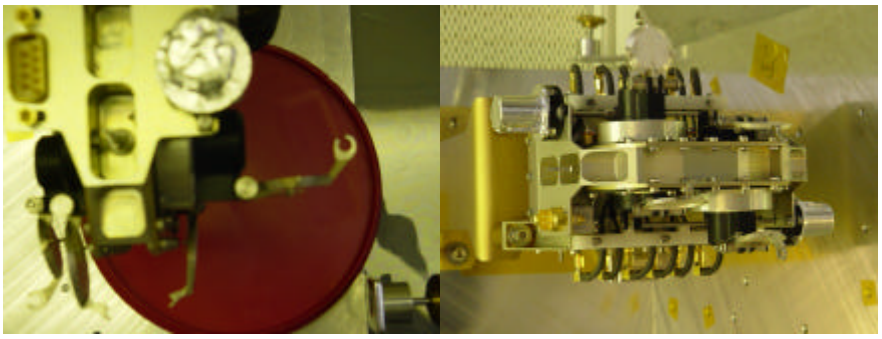

Figure 11: SEPT cover opening failure.

One cover did not fully open on SEPT-NS FM2 (pinpuller ref: 5069) proton channel after the vibration tests (see Figure 11 left: cover is in 3 o'clock position, should be in 6 o'clock position). On a second attempt after re-closing, the cover successfully opened. The reason for incomplete opening is not clearly understood, but one strong hypothesis is that the thermal coating (black anodize and Goddard composite) which has been applied on the cover rotation support may have increased the friction by getting loose during vibration. This hypothesis was supported by a close inspection of the collimator entrance on which the coating has been slightly removed at the areas of contact with the cover.

7 Conclusion

The four SEPT units were tested according to AD1. During random tests, active notching was used in certain cases with a maximum value of –2.57dB for SEPT-E X axis, so still within the +/-3 dB input tolerance. Comprehensive Performance Tests as defined in AD2 were carried out after each axis has been completed, no shift has occurred in the instrument response.

However, one failure occurred during cover opening which needs further attention.

Appendix

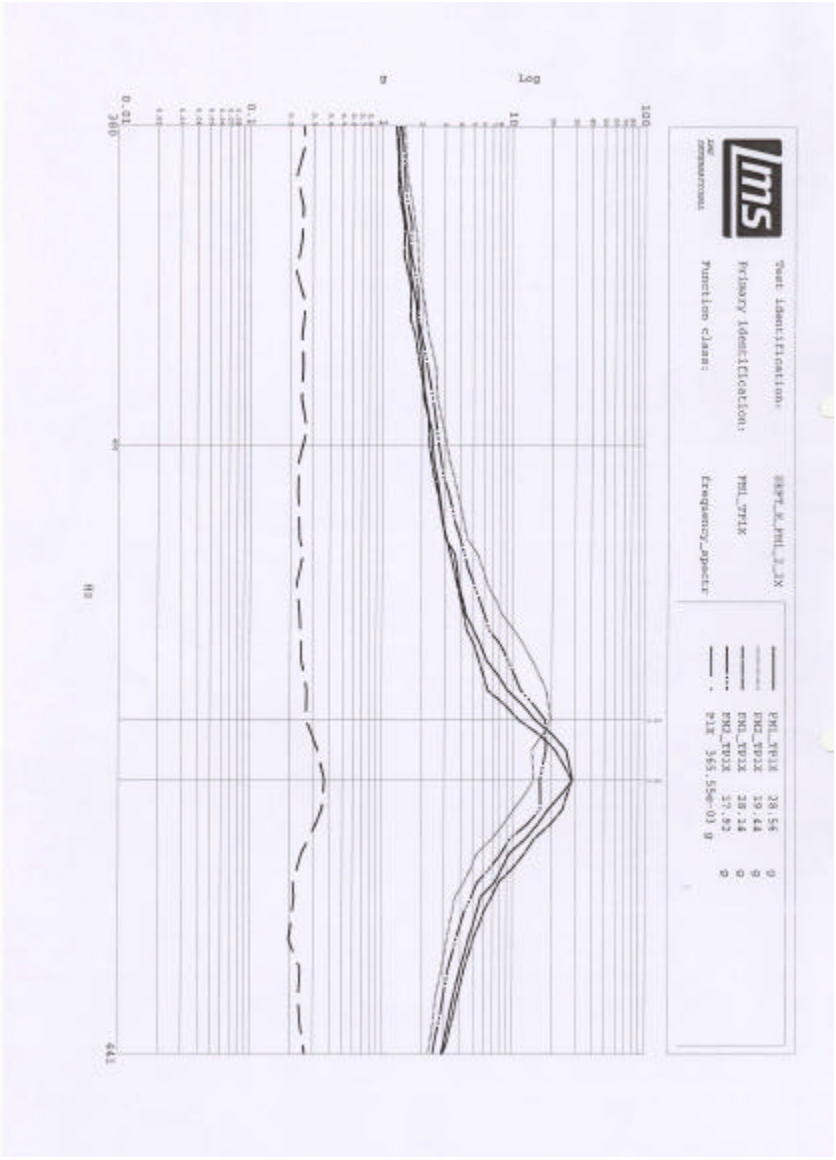

Figure 12 Example of input and output levels for calculations of the Q factor

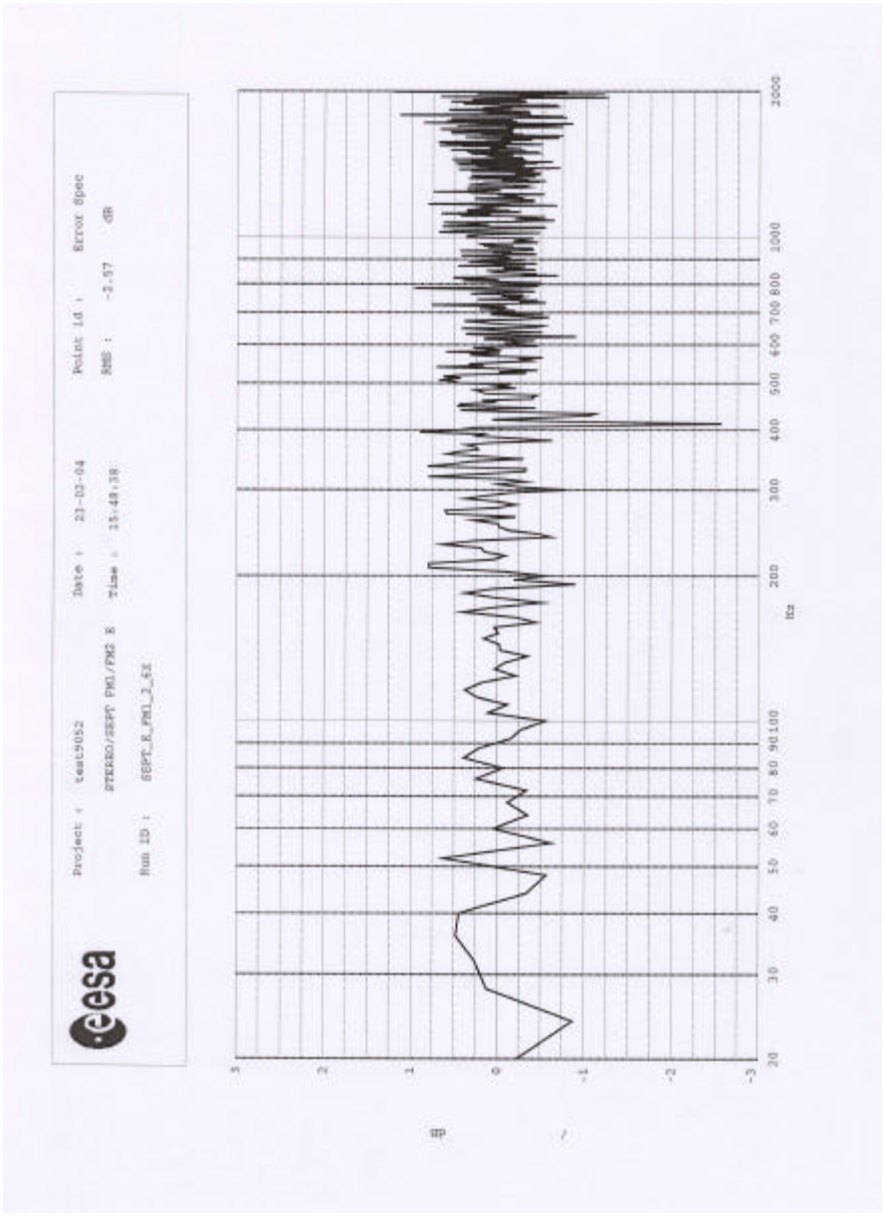

Figure 13 Typical error curve. In that case, the maximum error due to active notching happens at the resonance frequency and is -2.57 dB.

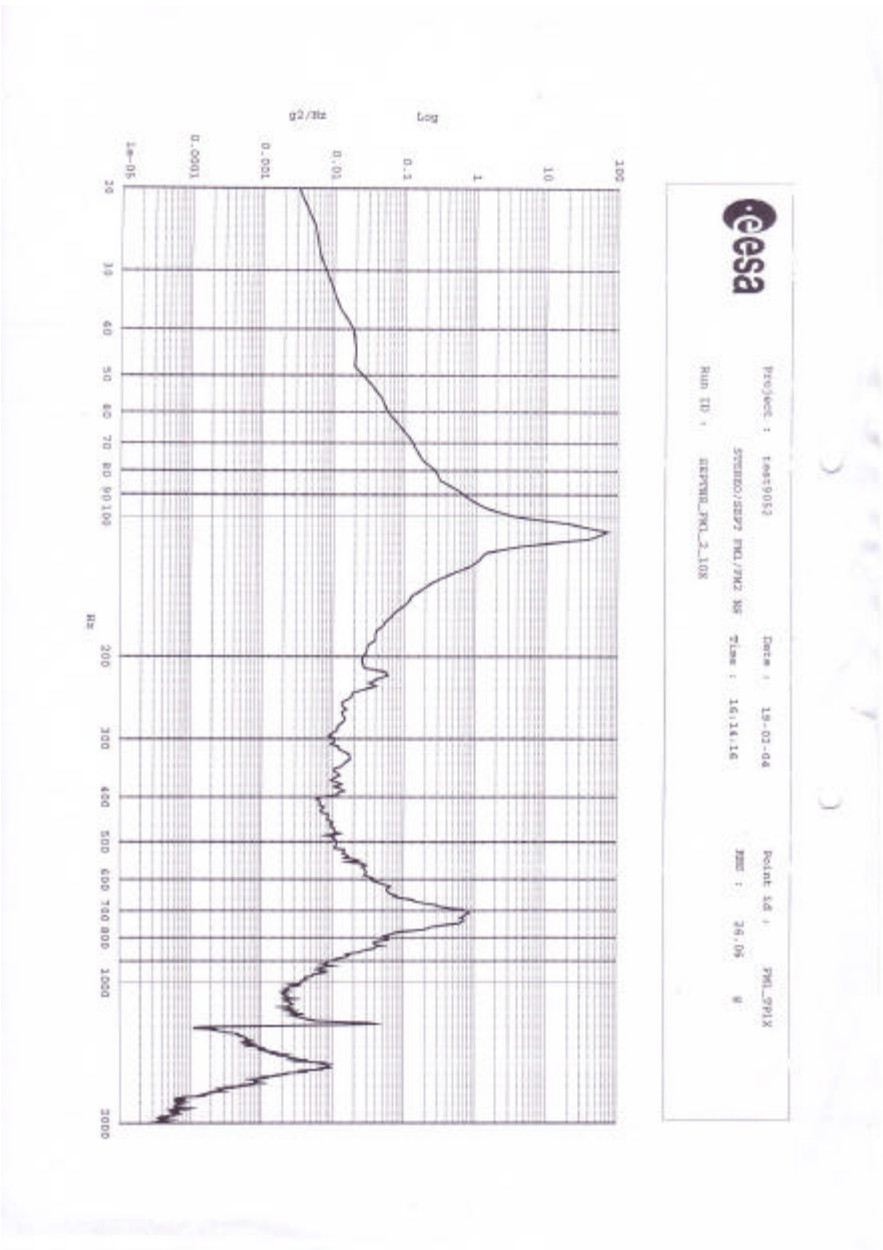

Figure 14 SEPT-NS FM1 X axis random

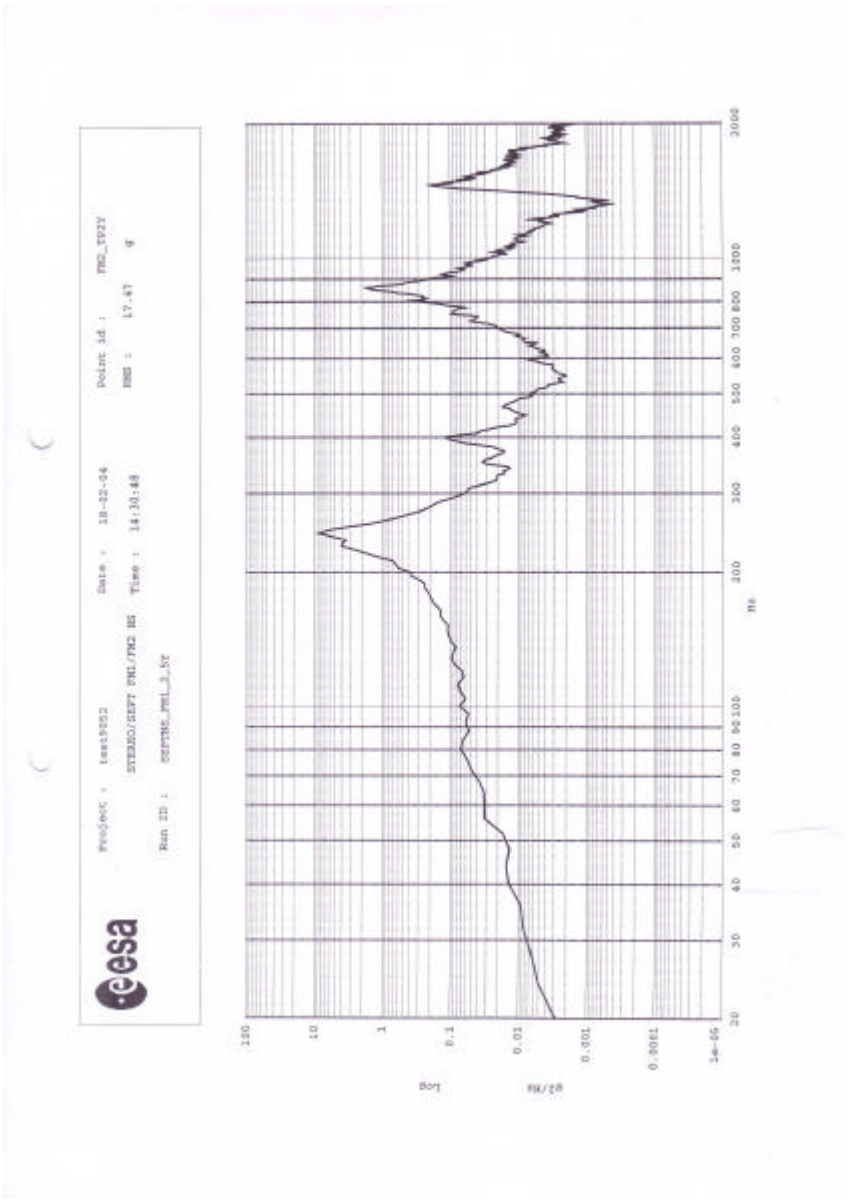

Figure 15 SEPT-NS FM1 Y axis random test

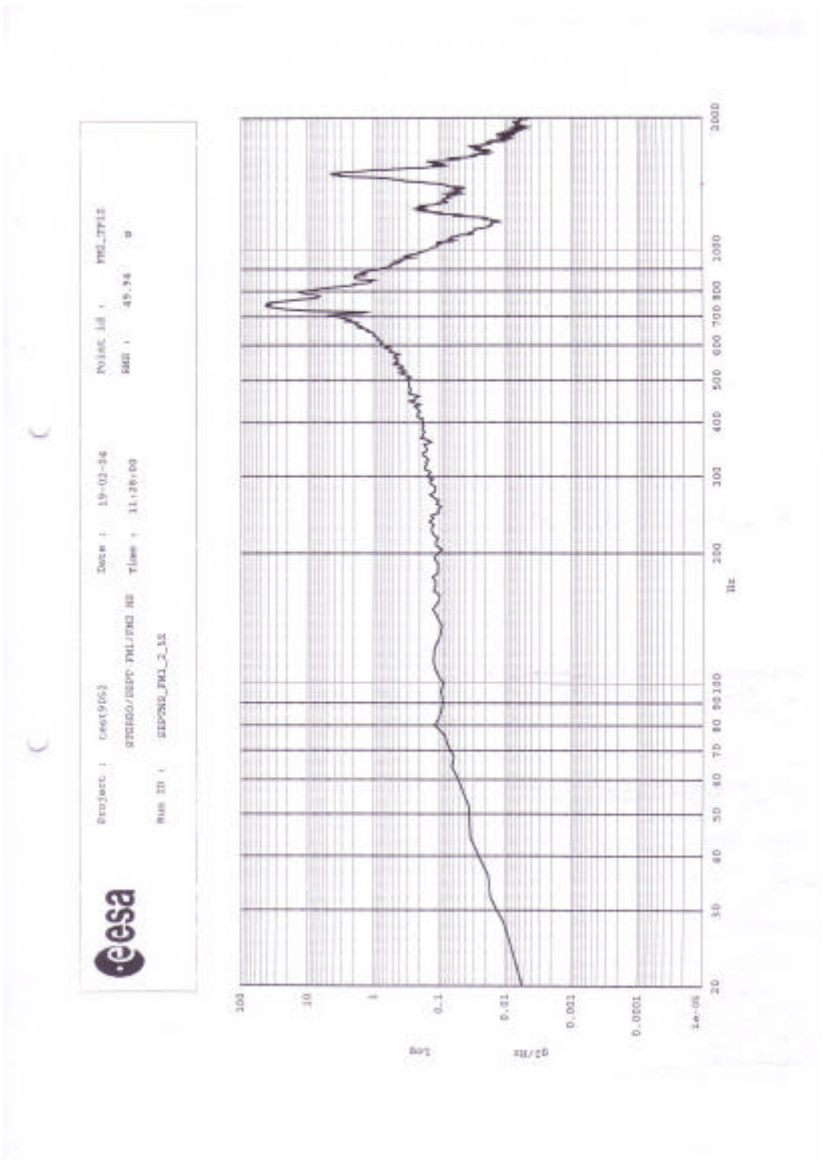

Figure 16 SEPT-NS FM2 Z axis random

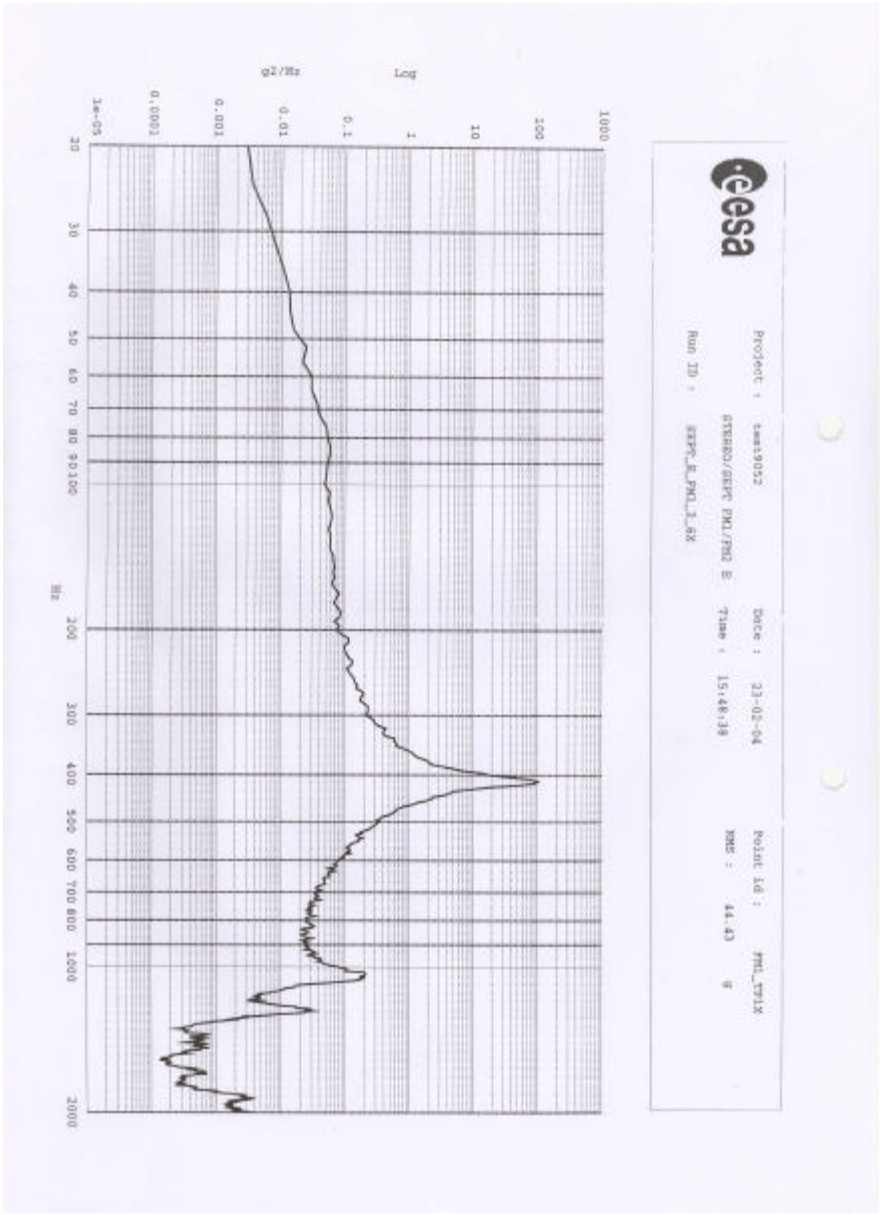

Figure 17 SEPT-E FM1 X axis random

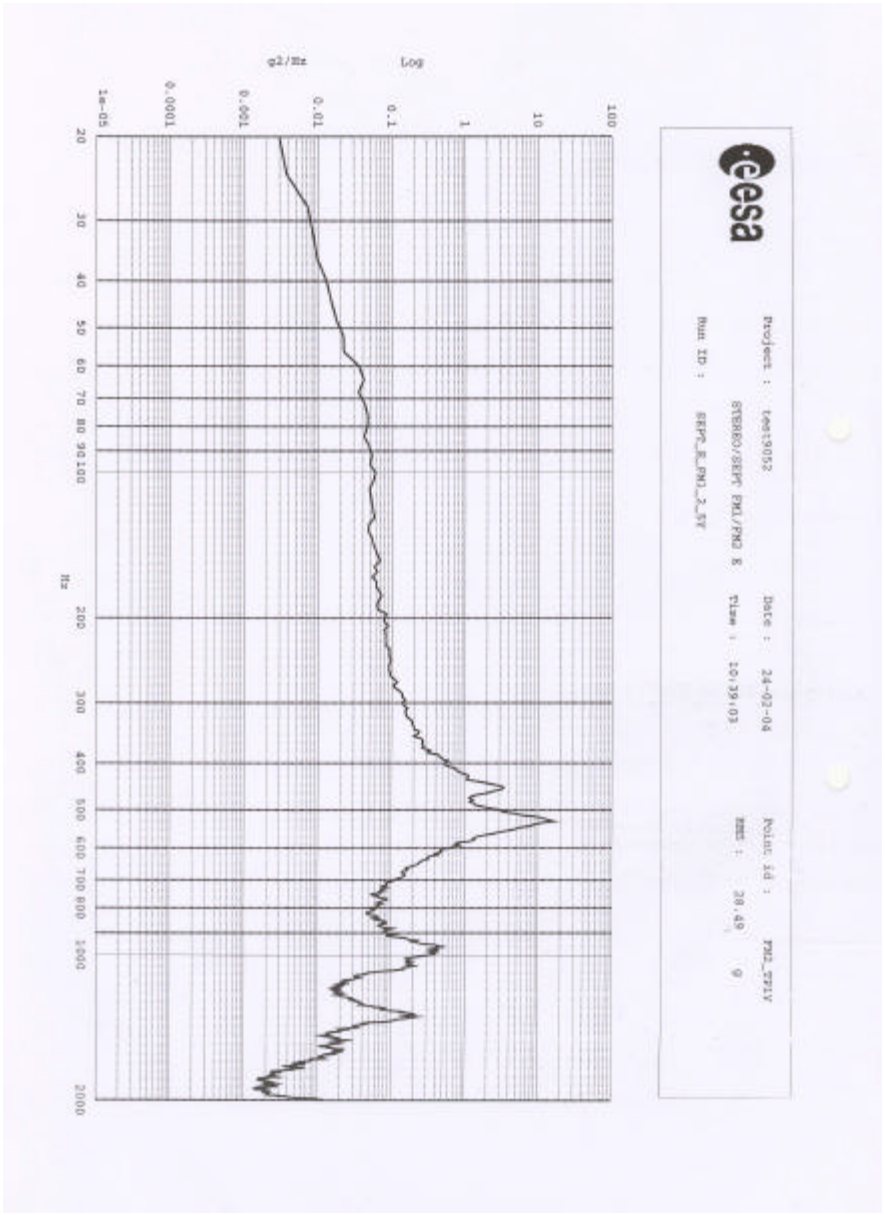

Figure 18 SEPT-E FM1 Y axis random

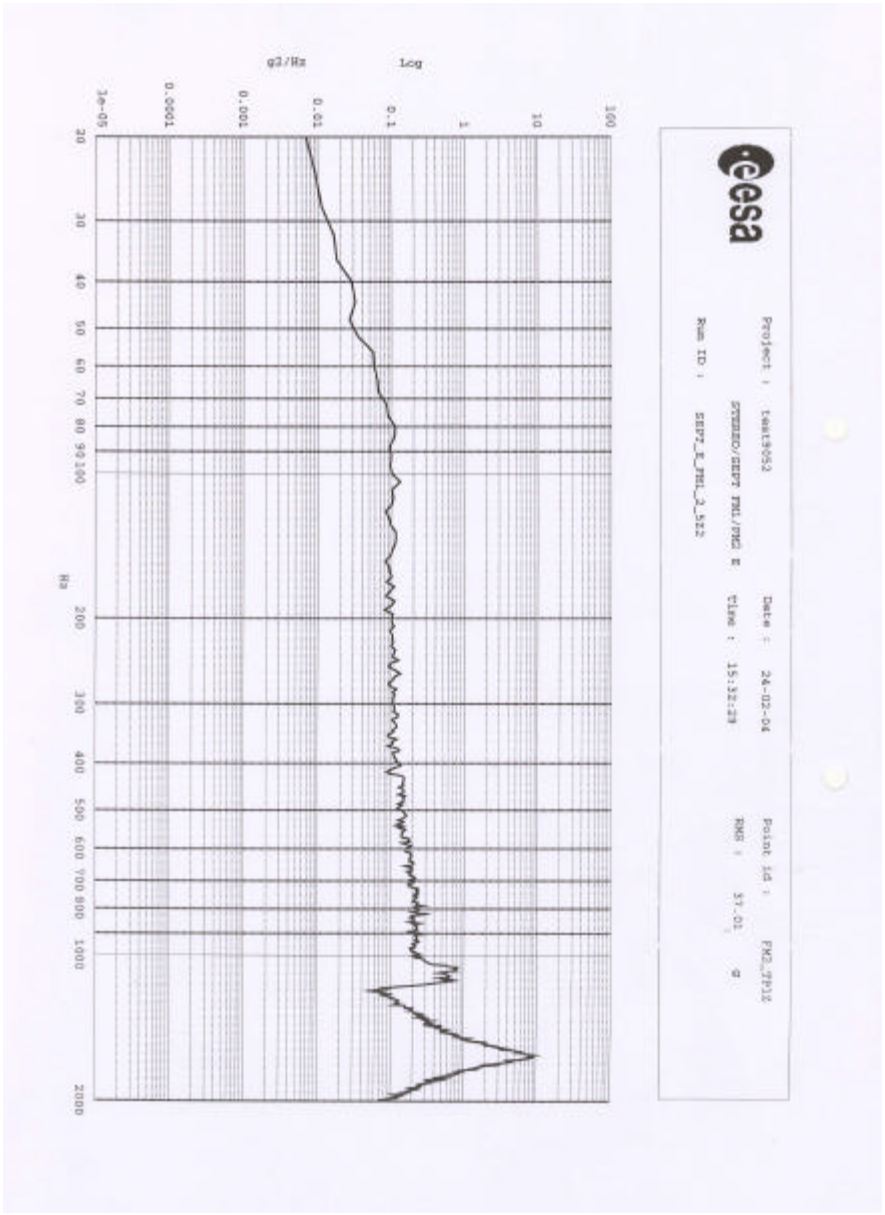

Figure 19 SEPT-E FM2 z axis